Article

Using Liquid Crystals to Reveal How Mechanical Anisotropy Changes Interfacial Behaviors of Motile Bacteria

Peter C. Mushenheim,[1] Rishi R. Trivedi,[2] Douglas B. Weibel,[2,*] and Nicholas L. Abbott[1,*]
[1]Department of Chemical and Biological Engineering and [2]Department of Biochemistry, University of Wisconsin-Madison, Madison, Wisconsin

ABSTRACT Bacteria often inhabit and exhibit distinct dynamical behaviors at interfaces, but the physical mechanisms by which interfaces cue bacteria are still poorly understood. In this work, we use interfaces formed between coexisting isotropic and liquid crystal (LC) phases to provide insight into how mechanical anisotropy and defects in LC ordering influence fundamental bacterial behaviors. Specifically, we measure the anisotropic elasticity of the LC to change fundamental behaviors of motile, rod-shaped *Proteus mirabilis* cells (3 μm in length) adsorbed to the LC interface, including the orientation, speed, and direction of motion of the cells (the cells follow the director of the LC at the interface), transient multicellular self-association, and dynamical escape from the interface. In this latter context, we measure motile bacteria to escape from the interfaces preferentially into the isotropic phase, consistent with the predicted effects of an elastic penalty associated with strain of the LC about the bacteria when escape occurs into the nematic phase. We also observe boojums (surface topological defects) present at the interfaces of droplets of nematic LC (tactoids) to play a central role in mediating the escape of motile bacteria from the LC interface. Whereas the bacteria escape the interface of nematic droplets via a mechanism that involved nematic director-guided motion through one of the two boojums, for isotropic droplets in a continuous nematic phase, the elasticity of the LC generally prevented single bacteria from escaping. Instead, assemblies of bacteria piled up at boojums and escape occurred through a cooperative, multicellular phenomenon. Overall, our studies show that the dynamical behaviors of motile bacteria at anisotropic LC interfaces can be understood within a conceptual framework that reflects the interplay of LC elasticity, surface-induced order, and topological defects.

INTRODUCTION

Many bacteria live at interfaces (1–11). The accumulation of bacteria at liquid-solid and liquid-air interfaces is an early step in the formation of bacterial communities that have a staggering impact on ecology (1–5), industrial processing (1,6,7), agriculture (1,8,9), and human health (1–3,5,10,11). In response to the growing significance attributed to bacteria in these niches, microbiologists have studied the mechanisms that influence cell movement, behavior, and assembly into multicellular structures at interfaces (12–17). Much of this research has centered around biofilms on the surfaces of rigid solids due to the impact of these structures on human health, and the high costs associated with eradicating these microbial communities (18–20). The extracellular matrix of biofilms (21–25) and other complex viscoelastic fluids in which bacteria live (e.g., synovial fluid, mucus, as well as fluids enriched in biopolymers such as collagen, chitin, and cellulose (15,26–31)) can possess local domains that exhibit long-lived anisotropic physical properties, particularly when they are exposed to shear or extensional flows. For instance, elastic relaxation times of bacterial biofilms, which commonly grow in flowing aqueous environments, have been measured to range from seconds to >10 min (21–25). Thus, motile bacteria associated with biofilms (32) come into contact with extracellular polymeric substance domains that exhibit local alignment. However, virtually nothing is known about how anisotropy of an interfacial environment impacts fundamental bacterial behaviors. Significantly, the range of bacteria living in these anisotropic environments includes the biomedically important organisms *Mycobacterium tuberculosis*, *Neisseria gonorrhoeae*, *Pseudomonas aeruginosa*, *Staphylococcus aureus*, and beta-hemolytic strains of *Streptococcus* (24,28,31). Although previous investigators have studied bacteria at interfaces of isotropic liquids (33–37), developing an understanding of the behavior and dynamics of bacteria at interfaces of anisotropic complex fluids, such as the liquid crystals (LCs) described in this work, has the potential to open a new window through which to view bacteria in environments that are relevant to biofilms, infections, and other fundamental and technological contexts.

In contrast to our lack of understanding of motile bacteria at the interfaces of complex fluids such as LCs, much more is known about the behavior at LC interfaces of synthetic microparticles that are commensurate in size to bacteria (38–45). Three key properties of LCs impact the equilibrium and dynamic interfacial behaviors of such micrometer-sized particles. First, because of the long-range ordering of molecules within LC phases, elastic strain of LCs about adsorbed microparticles gives rise to interparticle forces that have unusual symmetries (38–42). These LC-mediated interparticle forces can generate hexagonal and chain-like two-dimensional

Submitted February 6, 2014, and accepted for publication April 28, 2014.
*Correspondence: weibel@biochem.wisc.edu or abbott@engr.wisc.edu
Editor: Dennis Bray.

0006-3495/14/07/0255/11 $2.00
http://dx.doi.org/10.1016/j.bpj.2014.04.047

interfacial assemblies. Second, LC phases possess anisotropic viscosities that influence the dynamics of localized particles, as indicated by the anisotropic diffusion of microparticles adsorbed to LC interfaces (43). Third, topological defects that form at the surfaces of curved LC interfaces, such as LC droplets, possess high free energy densities and thus attract and localize microparticles (44,45). Inspired by these past observations regarding synthetic microparticles at LC interfaces, we hypothesized that LC elasticity, viscosity, and topological defects would also likely impact fundamental behaviors of motile bacteria at LC interfaces.

In this work, we report the use of *Proteus mirabilis* as a model bacterium to study the dynamics of motile bacteria at interfaces of LCs, as it has been demonstrated previously that genetically manipulating flagella density on *P. mirabilis* can create cells that produce sufficient flagella-derived propulsive forces to move through viscous fluids (46). Specifically, *P. mirabilis* cells overexpressing flagella (that we refer to as *P. mirabilis* in this work) are rod-shaped with a length of ~3 μm and move at a velocity, $\overline{V} = 6.9 \pm 1.6$ μm/s through an aqueous polymer solution that has a kinematic viscosity (0.83 Pa•s) (46) comparable to the nematic LCs reported in this work. The interfaces used in our studies of *P. mirabilis* are formed between coexisting isotropic and nematic domains of aqueous solutions of disodium cromoglycate (DSCG) (Fig. 1 *A*). This use of DSCG interfaces extends previous studies of bacterial motility within the bulk phase of the LC (47–49). Of particular relevance to this work, we recently reported that *P. mirabilis* cells align nematic DSCG phases parallel to their surfaces (48). Minimization of the associated elastic strain of the LC resulted in orientations and motions of the rod-shaped cells along the nematic director (48). We found also that the elasticity of the LC mediates attractive forces that assemble *P. mirabilis* cells into linear, multicellular structures. Formation of these structures was dynamic and reversible due to the interplay of flagella-derived propulsive forces and the elasticity-mediated attractive forces, both of which were comparable in magnitude for motile *P. mirabilis* cells (tens of pN).

The nematic-isotropic (N-I) interfaces used in our current study are defined by tactoids, which are elongated and cusped domains of either nematic LC in a continuous isotropic solution or isotropic phase domains dispersed in a continuous LC phase (50–53). Such domains define a particularly interesting class of LC interfaces because their geometry leads to the generation of surface-localized topological defects (see below for additional discussion). Using this experimental system, we sought to determine whether bacteria would insert into the N-I interface of the tactoids and whether the orientational order (and associated anisotropic mechanical properties) of the nematic interface would guide the interfacial motility of cells. In addition, inspired by observations (see above) of the association of microparticles with defects of LC droplets (44,45), we aimed to explore how motile bacteria would be influenced by interfacial defects in the LC order. As described below, we find that the nematic elasticity of the LC combines with the presence of defects to define specific pathways by which bacteria can escape from nematic interfaces. We also show how this phenomenon can be tuned to control the capture and release of motile bacteria in LCs. We close this Introduction by noting that a recent publication by Zhou et al. reports an observation regarding the interaction of *Bacillus subtilis* cells with isotropic tactoids in nematic LC (49). Below we contrast our findings with *P. mirabilis* to the observation with *B. subtilis* cells.

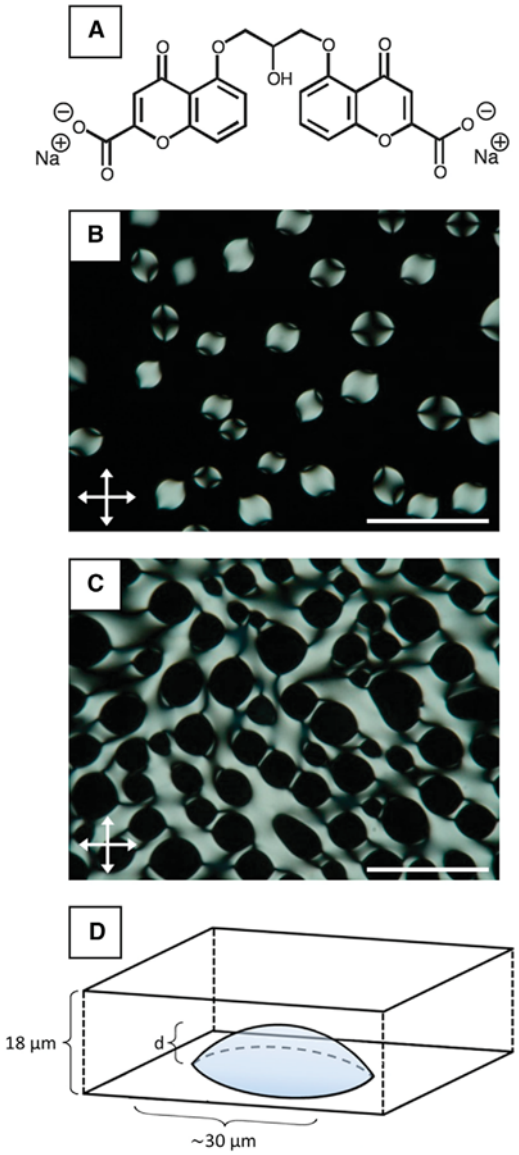

FIGURE 1 Formation of nematic and isotropic tactoids. (*A*) Molecular structure of DSCG. (*B* and *C*) Crossed polar images of (*B*) nematic and (*C*) isotropic tactoids. The nematic tactoids formed in imaging chambers following cooling of an isotropic phase of 15 wt % DSCG solution from 40°C to 33°C; isotropic tactoids formed in imaging chambers following heating of a nematic phase DSCG solution from 25°C to 30°C. (*D*) Three-dimensional depiction of the shape adopted by sessile tactoids (both isotropic and nematic) in our experiments. Scale bars are 100 μm. To see this figure in color, go online.

MATERIALS AND METHODS

Bacterial strains and cell culture

P. mirabilis strain HI4320 was transformed with plasmid pflhDC to create *P. mirabilis* cells overexpressing flagella. The plasmid pflhDC contained the *flhDC* genes from *P. mirabilis* inserted into pACYC184 (which contains a gene for chloramphenicol resistance). *P. mirabilis* cells were grown in chloramphenicol-resistance nutrient medium consisting of 1% (wt/vol) peptone (Becton, Dickinson, Sparks, MD), 0.5% (wt/vol) yeast extract (Becton, Dickinson), and 1% (wt/vol) NaCl (Fisher Scientific, Fairlawn, NJ) at 30°C in a shaking incubator (46). Saturated overnight cultures were diluted 100-fold in 10 mL of fresh nutrient medium and grown in 150 mL Erlenmeyer flasks at 30°C in a shaking incubator at 200 rpm. We observed that the highest swimming velocity of *P. mirabilis* cells occurred during the stationary phase, hence we harvested cells at an absorbance ($\lambda = 600$ nm) of ~3.2 and concentrated them by centrifugation. The cells were washed three times with an aqueous buffer for bacterial motility (0.01 M KPO_4, 0.067 M NaCl, 10^{-4} M EDTA, 0.1 M glucose, and 0.001% Brig-35, pH 7.0). To obtain nonmotile *P. mirabilis* cells, the cells were treated with 4% glutaraldehyde for 3 h at 25°C after harvesting.

Lyotropic LC preparation

DSCG was purchased from Sigma-Aldrich (Milwaukee, WI) and used as received. Lyotropic LCs containing DSCG were prepared by mixing 15.3 wt % of DSCG with 84.7 wt % of aqueous motility buffer. The mixture was shaken for at least 12 h to ensure complete solubility and homogeneity. Before experimentation, the DSCG solution was heated at 65°C for 10 min to avoid possible time dependence of the properties of the mixture (54,55). After cooling the solution to 25°C, a small volume of motility buffer containing bacteria was added to the DSCG mixture producing a final concentration of ~10^5 cells/μL. The final concentration of DSCG was 15.0 wt % in all experiments.

Preparation of imaging chambers

We created imaging chambers by adding a small volume (~1 μL) of DSCG solution on top of a glass slide between two sheets of 18 μm-thick Mylar film. A glass coverslip was placed on top of the Mylar and the chamber was sealed with epoxy to prevent water evaporation (see Fig. S1 in the Supporting Material). We confirmed the direction of alignment of the nematic LC by inserting a quarter wave plate into the optical path of a microscope and analyzing the appearance of the sample between crossed polars (56). Imaging chambers were used within 3 h of their preparation.

Microscopy

We imaged cells using a Nikon Eclipse Ti inverted optical microscope equipped with crossed polarizers and a Photometrics CoolSNAP HQ2 CCD camera (Tucson, AZ) using a Nikon Plan Apo λ, 100X/1.45 oil objective lens. Videos were collected with the electron multiplying gain off and with a 90 ms exposure time (11 frames/s). Images of cells were collected using Nikon NIS Elements software. A thermoplate (Tokai Hit, Fujinomiya, Japan) and 100X objective heater (Bioptechs, Butler, PA) were used to control the temperature of the samples during experiments. DSCG solutions were equilibrated at a particular temperature for at least 10 min before making observations and performing measurements of bacteria motility. An Olympus BX60 microscope equipped with crossed polarizers was also used to analyze the imaging chambers. Images were captured using a digital camera (Olympus C-2040 Zoom) mounted on the microscope and set to an f-stop of 2.8 and a shutter speed of 1/125 s.

Bacterial motility data analysis

Microscopy data for motile cells were analyzed using the MATLAB computing environment (The MathWorks, Natick, MA) by identifying the centroid of each bacterium in successive frames and grouping those points together to create a cell trajectory. These data were combined with the charge-coupled device frame rate to determine cell velocity.

Tactoid triple phase contact line measurement

Individual video frames were opened in ImageJ and the position of the triple phase contact line was determined using the Find Edges tool. Three consecutive traces of the triple phase contact line were performed to estimate its length.

Statistical analysis

All experimentally determined values have been reported in the text and figures with associated standard errors unless otherwise noted.

RESULTS

Capture and escape of *P. mirabilis* cells from the interfaces of nematic tactoids

We first sought to determine whether motile *P. mirabilis* cells would adsorb to interfaces formed between coexisting aqueous nematic and isotropic phases of 15 wt % DSCG in motility buffer. To this end, we prepared optical chambers containing 18 μm-thick DSCG films (see above) in which the nematic phase of DSCG was oriented parallel to the glass substrates and exhibited a degenerate azimuthal alignment. We observed the 15 wt % DSCG solution to form coexisting nematic and isotropic domains at temperatures between 29°C and 35°C. Specifically, after quenching samples from 40°C (isotropic phase) to 33°C, spindle-like domains of nematic phase with positive interface curvature and an elongated and cusped shape (tactoids) formed on the surface of the glass slides within a continuous isotropic phase (Fig. 1 *B*) (50–53). The prolate shape of the tactoids arises from a competition between the elasticity of the nematic phase and the interfacial tension between the nematic and isotropic phases (57,58). As detailed elsewhere (50–53), imaging of the nematic tactoids between crossed polars confirmed that the LC was anchored tangentially at the N-I interface and that two topological LC defects (boojums (50,59)) were located at the cusped poles near the triple phase (N-I-glass substrate) contact line. Although the elastic constant for twist (K_{22}) in nematic DSCG is an order of magnitude smaller than the elastic constants for splay (K_{11}) and bend (K_{33}) (60), we did not observe a twisted director profile within the sessile nematic tactoids, as evidenced by the extinction that occurs in the center of the tactoid when the major axis of the tactoid is aligned parallel with one of the polarizers (Fig. 1 *B*) (51,52,57,61,62). We also formed isotropic phase tactoids (in a continuous nematic phase) in our studies by heating a 15 wt % DSCG

solution from 25°C (nematic phase) to 30°C (Fig. 1 *C*). We observed that both nematic and isotropic tactoid domains generally nucleated at and remained attached to one of the glass substrates and following equilibration at either 33°C (nematic tactoids) or 30°C (isotropic tactoids) for several minutes, grew to a structure that was 30-μm in diameter along the major axis (Fig. 1 *D*). Unless otherwise noted, we restrict our observations to tactoids that had depth $d < 18$ μm, which is smaller than the gap between the glass substrates.

When *P. mirabilis* cells were dispersed uniformly in isotropic phases of DSCG at 40°C and then cooled to 33°C, we observed that the cells were excluded from the growing nematic domains (Figs. 1 *B* and 2 *A*) and became concentrated in the continuous isotropic phase as well as proximate to the curved N-I interfaces of the tactoids. The *P. mirabilis* cells suspended within the bulk isotropic phase at 33°C moved without a directional bias with an average velocity of $\overline{V} = 17.6 \pm 0.7$ μm/s ($N = 34$), which is significantly faster than the velocity we measured previously for *P. mirabilis* cells in an isotropic phase of 15 wt % DSCG at 42°C ($\overline{V} = 8.1 \pm 0.3$ μm/s (48)) (Table 1). This difference in velocity is consistent with an increase in the viscosity of isotropic DSCG solutions with decreasing temperature (54) and an inverse relationship between *P. mirabilis* velocity and solution viscosity for $\mu < 9$ mPa•s (46) (See Table 1 for viscosities). In contrast to the random movement of cells in the bulk isotropic phase, we observed bacteria near the surface of tactoids propelling themselves with clear directional bias along the N-I interface and the triple phase contact line with an average velocity of $\overline{V} = 17.1 \pm 0.4$ μm/s ($N = 40$) (Table 1). We discuss the magnitude of this interfacial velocity and origin of the biased motion below.

Limited by the resolution of our optical microscope, we were unable to initially determine whether the *P. mirabilis* cells near the N-I interface were inserted into the interface, such that they contacted both nematic and isotropic phases, or whether they remained suspended in the isotropic phase.

TABLE 1 Velocity of *P. mirabilis* in bulk DSCG phases and N-I interfaces

Location	Temperature	Estimated viscosity (mPa•s)	Velocity (μm/s)
Bulk nematic	25°C	700[a]	8.8 ± 0.2[b]
Bulk nematic	30°C	650[a]	9.5 ± 0.6
Bulk isotropic	33°C	9[c]	17.6 ± 0.7
Bulk isotropic	42°C	2[c]	8.1 ± 0.3[b]
N-I interface (isotropic tactoid)	30°C		16.7 ± 0.5
N-I interface (nematic tactoid)	33°C		17.1 ± 0.4

[a]Estimated based on comparison of velocity of *P. mirabilis* cells in 15 wt % DSCG to previous measurements (46) of *P. mirabilis* motility in isotropic solutions of known viscosity.
[b]Data taken from (48).
[c]Estimated based on measurements of the shear viscosity of aqueous solutions of 14 wt % DSCG (54).

We hypothesized that if they were inserted into the interface, *P. mirabilis* cells (which we reported previously anchor LCs tangentially (48)) would preferentially orient and move parallel to the local director at the interface of the tactoid due to the elasticity of the nematic phase. Fig. 2 *C* depicts the trajectory of a *P. mirabilis* cell that we observed to move along the N-I interface of a nematic tactoid. The cell depicted in Fig. 2 *C* moves out of the focal plane—located at the surface of a glass slide—as it moves along the interface of the sessile tactoid. A comparison of Fig. 2, *B* and *C*, reveals that the trajectory of the cell follows the interfacial director profile of the tactoid (Movie S1). We also determined the long axis of the motile bacterium to be oriented parallel to the LC director. Analysis of additional bacterial trajectories near nematic tactoids yielded similar results (Fig. S2). In particular, we note that due to the quadrupolar symmetry

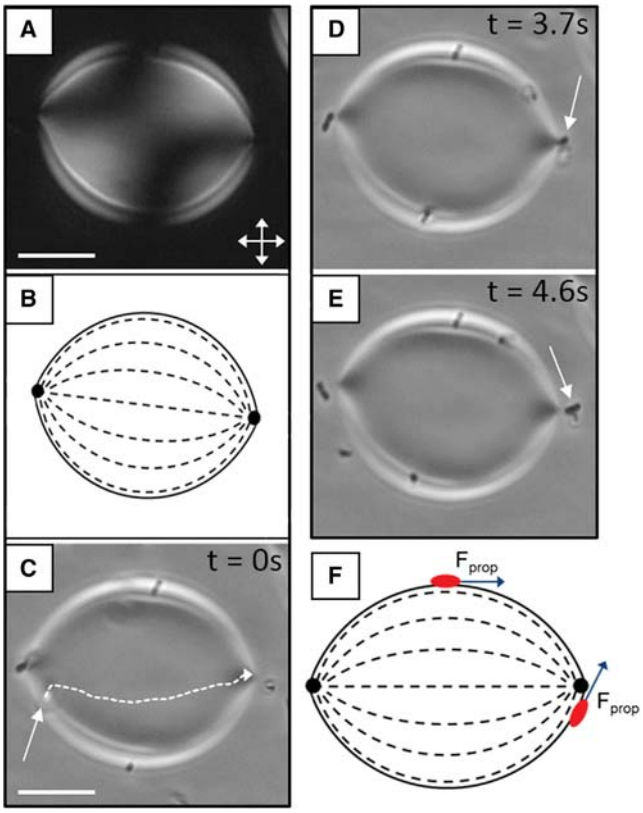

FIGURE 2 Guided motility and escape of a cell adsorbed to a nematic tactoid. (*A*) Optical micrograph (*crossed polars*) of a nematic tactoid that formed within a continuous isotropic phase upon quenching a 15 wt % DSCG sample from 40°C to 33°C and that partially wets one of the glass surfaces of the imaging chamber. (*B*) Schematic representation of the LC director profile of the tactoid in *A*. (*C*) Bright field micrograph of a nematic tactoid on which the trajectory of a motile *P. mirabilis* cell (depicted by an *arrow*) adsorbed to the N-I interface is indicated. (*D* and *E*) Bright field micrographs of a motile cell that escapes from the N-I interface at a boojum (*topological defect at the cusped pole*) of the tactoid. In *D*, the cell is oriented toward the viewer. (*F*) Schematic diagram depicting the orientation of the flagella-derived propulsive force (F_{prop}) of motile bacteria adsorbed at various positions on the interface of a nematic tactoid. Scale bars are 10 μm. To see this figure in color, go online.

of the tactoids, bacteria were guided by the LC director toward either of the boojum defects. Based on the directed motion of *P. mirabilis* at the interface of the tactoid, we concluded that the motile cells adsorb and insert into the N-I interface. We also observed nonmotile bacteria (*P. mirabilis* cells treated with 4% glutaraldehyde) to adopt orientations parallel to the local nematic director when positioned at the interface of nematic tactoids (Fig. S3).

The strong adsorption of micrometer-sized particles to liquid-liquid interfaces is known to be driven, in part, by the interfacial tension between the two phases. To determine if the interfacial tension between the isotropic and nematic phases of the DSCG solution (γ_{NI}) is sufficiently large to drive the adsorption of the bacterial cells, we considered that the prolate shape of tactoids (with characteristic radius, R) arises from a balance between the elasticity of the bulk nematic phase (which scales as ~KR, where K is a one constant approximation of the LC elastic constant) and the energy of the N-I interface (which scales as $\gamma_{NI}R^2$) (51,57,58). For these bulk and surface energies to be comparable when R ~10^{-5} m (using K ~10 pN (60)), we estimate that γ_{NI} is ~10^{-6} J/m^2. This agrees with estimates of γ_{NI} for other lyotropic LCs including aqueous sols of vanadium pentoxide (57) (γ_{NI} ~10^{-6} J/m^2) and aqueous suspensions of cellulose crystallites (63) (γ_{NI} ~10^{-6} – 10^{-7} J/m^2) although a larger estimate (γ_{NI} ~10^{-4} J/m^2) has been reported previously for DSCG (50). By modeling *P. mirabilis* cells as rod-shaped particles with a major axis 2*a* and minor axis 2*b*, and by noting the radius of curvature of the interface to be large compared to the cell, the interfacial area (A_{NI}) removed due to the presence of an adsorbed bacterium is given by $A_{NI} = \pi b^2 \sin^2[\cos^{-1}(1 - h/b)][1 + ((4(a/b - 1))/(\pi \sin[\cos^{-1}(1 - h/b)]))]$, where h is the depth of immersion of the bacterium in the nematic phase (64). From this expression, we calculate the maximum area occupied by *P. mirabilis* to be 2.8 μm^2, thus leading to an upper bound on the contribution of γ_{NI} to the adsorption energy of 3 × 10^{-18} J/cell (~10^3 kT). This value is consistent with our observation of irreversible adsorption of nonmotile *P. mirabilis* cells to the interfaces of nematic tactoids of DSCG.

Although we calculated *P. mirabilis* cells to be attached to the N-I interface with an adsorption energy of ~10^3 kT, we observed motile cells to be able to escape from the interface of nematic tactoids and enter the continuous isotropic phase. Fig. 2, *C–E*, show a representative example in which a motile cell adsorbs to a nematic tactoid and follows the director profile along the interface of the tactoid (Fig. 2 *C*) to arrive at one of the two cusped poles of the tactoid, where a boojum is present (Fig. 2 *D*). At the boojum, the cell escapes from the N-I interface into the isotropic phase (Fig. 2 *E*). Overall, we found that two-thirds ($N = 170$) of motile bacteria that escaped from the interface of nematic tactoids did so near a boojum. We hypothesize that this dominant mode of escape reflects the fact that i), motile bacteria are focused to the boojums by the convergence of the LC director profile (Fig. 2 *B*); and ii), a component of the flagella-derived force produced by cells (F_{prop}; estimated to be ~60 pN for *P. mirabilis* moving in bulk nematic DSCG (48)) is directed normal to the contact line near the boojum and thus can overcome forces associated with interfacial tension that hold cells at the interface (Fig. 2 *F*). These ideas are supported by additional observations reported below, which reveal motile bacteria to escape from the N-I interfaces of isotropic tactoids almost exclusively via boojums.

Whereas bacterial cells were able to escape from the N-I interface into the isotropic phase, we did not observe detachment of motile bacteria from the N-I interface into the interior of the nematic tactoids in our experiments. We hypothesize that an energetic penalty associated with elastic strain of the nematic director around a cell, which occurs principally near the hemispherical poles of the bacteria (48,65), is likely responsible for this observation and will tend to prevent escape of bacteria into the LC phase. We estimate the energy associated with the elastic strain of the LC around a cell on the interface as $E_{elastic} \sim Kb\, f(h/b)$, where $f(x)$ is a dimensionless function of the location of the cell at the interface (40,66). For *P. mirabilis* and 15 wt % DSCG, we estimate Kb to be 5 × 10^{-18} J, and conclude that the magnitude of this elastic energy penalty is comparable to the adsorption energy due to interface tension. We note that we estimate the energy associated with the extension of the N-I interface around an adsorbed cell due to capillary deformations to be only on the order of 10^{-20} J (67), and thus small compared to the elastic energy associated with strain of the LC.

The previous conclusion that the energetic effects associated with elastic deformations around bacteria are comparable to interfacial tension leads us to also hypothesize that the nematic elasticity of the LC likely impacts the location of cells at N-I interfaces. Specifically, the elasticity of the LC should promote contact of the surface of the cells with the isotropic phase at the interface. Indeed, our measurement of *P. mirabilis* cells moving along the N-I interface with an average velocity similar to that in bulk isotropic phase at 33°C (Table 1) suggests that the majority of the surface of each cell is in contact with the isotropic phase.

Dynamics of *P. mirabilis* cells at the interfaces of isotropic tactoids

Based on the previous observations, we interpret the elasticity of the LC and the presence of topological defects to play key roles in influencing the interfacial behavior of bacteria. To further explore how these properties of the N-I interface impact *P. mirabilis* behaviors, we created isotropic domains within a continuous nematic phase by heating 15 wt % DSCG solutions from 25°C (*nematic phase*) to 30°C (Fig. 1 *C*). The lateral size (~30 μm in diameter) and elongated, tactoidal shape of the isotropic domains resembled

the nematic tactoids at 33°C described previously. However, tangential anchoring of the LC produced boojum defects just outside the N-I interface of the two cusped poles of the isotropic tactoids (Fig. 3, *A* and *B*). In addition, the morphologies of the isotropic domains that formed—particularly when they were in close proximity to one another (Fig. 1 *C*)—displayed considerably greater complexity than the nematic domains (Fig. 1 *B*) due to the strain present in the continuous nematic phase separating the isotropic domains. We found that isotropic domains with either one or three cusps nucleated from the cores of half-integer disclinations when heating from the nematic phase (50). Below, we describe experiments with motile bacteria interacting with sessile isotropic tactoids containing two cusps.

During the heating of DSCG solutions into the biphasic region, we observed motile *P. mirabilis* cells adsorb to the interface of the growing isotropic tactoid domains. Consistent with previous observations for *B. subtilis* (49), the orientation and motion of the adsorbed motile *P. mirabilis* cells were constrained to be parallel to the orientation of the local director of the adjacent nematic phase (Fig. 3, *B* and *C*), similar also to motile bacteria adsorbed to nematic tactoids (Fig. 2). Cells moved along the interface of isotropic tactoids with an average velocity of $\overline{V} = 16.7 \pm 0.5$ μm/s ($N = 40$). This velocity is similar to our measurement of bacterial motility at the interface of nematic tactoids (Table 1) and suggests that the interfacial environment experienced by *P. mirabilis* cells at the N-I interface (away from the cusps) is similar for the two types of tactoids.

In contrast to our observations with nematic tactoids (motile cells did not detach from the N-I interface to enter the nematic phase), however, we observed motile *P. mirabilis* cells to escape the N-I interface of isotropic tactoids into the surrounding nematic phase. Escape of motile cells into the nematic phase primarily (~95%, $N = 274$) occurred at one of the two cusped poles of the tactoid, where boojums are located in the adjacent nematic phase (Fig. 3 *B*). We observed cell detachment to occur by at least two mechanisms. First, as shown by the sequence of micrographs in Fig. 3 *C*, we observed individual *P. mirabilis* cells adsorbed at the N-I interface to move toward one of the cusps of the isotropic tactoids, where they escaped (Movie S2). Detachment of isolated cells from isotropic tactoids in this manner closely resembled our previous observations of the method of cell detachment from nematic tactoids (Fig. 2) as well as the mechanism of single-cell escape from the interface of an isotropic tactoid observed for *B. subtilis* (49).

However, we more frequently observed a second mechanism through which groups of motile *P. mirabilis* cells collectively escaped the interface of isotropic tactoids (Fig. 3 *D*, Movie S3). This event occurred when an adsorbed motile cell arrived at the cusp of an isotropic tactoid and appeared to get trapped by the boojum defect. Subsequently, additional cells that were directed toward the same cusp by the interfacial LC director profile were blocked in their escape by the

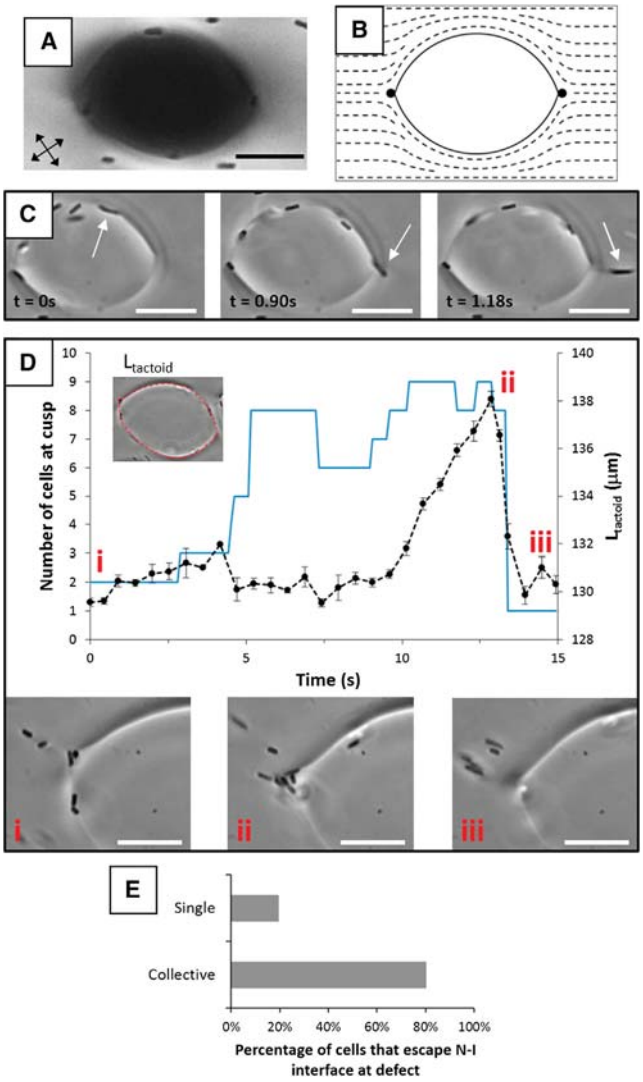

FIGURE 3 Escape mechanisms of motile bacteria from adsorption to an isotropic tactoid. (*A*) Optical micrograph (*crossed polars*) of a sessile isotropic tactoid that forms within a continuous nematic phase after heating a 15 wt % DSCG sample from 25°C to 30°C. (*B*) Schematic representation of the LC director profile in the nematic phase. (*C*) Sequence of images (*bright field*) depicting the escape of a motile *P. mirabilis* cell (indicated by an *arrow*) from the interface of an isotropic tactoid into the continuous nematic phase at the cusped pole of the tactoid (*adjacent to a boojum defect in the nematic phase*). (*D*) Graph and sequence of images (*bright field*) depicting the accumulation of motile *P. mirabilis* cells near the cusped pole of an isotropic tactoid and their collective escape. In the graph, the number of cells localized at the cusp is given by the blue line, whereas measurements of $L_{tactoid}$, the triple phase (N-I-glass substrate) contact line of the tactoid are given by the black data points (with a *dotted black line to guide the eyes*). The force generated by trapped cells at the pole deforms the interface and extends the triple phase contact line. Ejection of the trapped cells into the nematic phase allows the interface to relax to its initial shape. (*E*) A plot of the frequency with which motile cells escape the N-I interface of isotropic tactoids near defect points as either single cells (as in *C*) or through a collective mechanism (as in *D*). Scale bars are 10 μm. Error bars represent standard deviations. To see this figure in color, go online.

first cell. This phenomenon led to the accumulation of an assembly of cells at the boojum. After several cells were trapped near the boojum, these cells along with additional motile cells that arrived at the cusp exerted a collective force on the interface of the tactoid that was observed to deform the N-I interface near the accumulated cells and lead to a growing, measurable extension of the triple phase contact line with time (Fig. 3 *D*). Ultimately, after the N-I interface near the cusp had been significantly deformed, the arrival of one additional motile cell at the cusp was typically observed to initiate collective escape of the entire cluster of cells into the nematic phase. We measured the average colony size to lead to escape to be 4 cells, although as many as 10 or as few as two cells can also lead to escape. Free from the strain generated by the assembly of bacteria, the N-I interface relaxed back to its initial state and the process could be repeated. Overall, we found that motile *P. mirabilis* cells exited the N-I interface of isotropic tactoids much more frequently through this cooperative mechanism than as individual cells (Fig. 3 *E*). We also note that our observation of the trapping of motile bacteria at boojum defects near the cusps of isotropic tactoids closely resembles the partitioning of synthetic (e.g., polystyrene) microparticles to surface-associated defects of LC droplets (44,45). This latter phenomenon is driven by replacement of the high-energy defect core and surrounding strained LC by the particle. We hypothesize that this same mechanism underlies the trapping of motile bacteria at defects described in this work. In support of this hypothesis, we observed that nonmotile *P. mirabilis* cells, which adsorb irreversibly to isotropic tactoids, were also frequently localized at the cusps (Fig. S4). It is likely that elastic forces drive the localization of the nonmotile cells to the boojum defects near the cusps (44,45).

Although motile cells did not detach into the interior of nematic tactoids, we occasionally observed the detachment of motile cells into the interior of isotropic tactoids (Fig. S5). Together, these observations reflect the relative ease with which cells can detach from the N-I interface into the isotropic phase, likely due to several factors including the release of elastic strain accompanying cells at the interface (as opposed to introduction of additional strain associated with escape into the nematic phase) and the preferential wetting of adsorbed cells by the isotropic phase. To confirm this conclusion, we prepared two LC samples in parallel containing equal densities of motile cells. One sample was heated from room temperature to 30°C to form isotropic tactoids, whereas the other was cooled from 40°C to 33°C to form nematic tactoids. After equilibration for 15 min, we imaged many tactoids in both samples and quantified the number of motile bacteria found adsorbed to the N-I interface. The tactoids that we analyzed were all of similar size (~30 μm in diameter). Inspection of Fig. 4 reveals that cells were only concentrated on the interface of the isotropic tactoids (see also Fig. S6). Additional observations confirmed that motile *P. mirabilis* cells have a much shorter residence

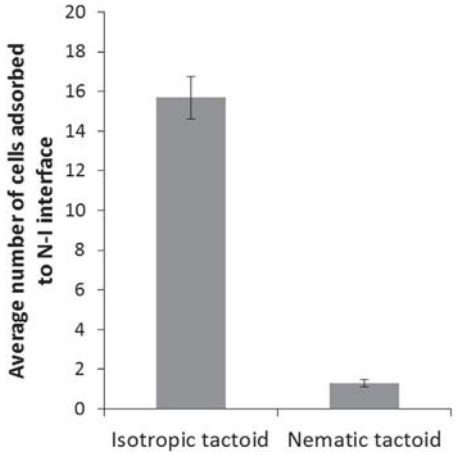

FIGURE 4 Temporal accumulation of motile bacteria at the interface of isotropic tactoids. Average number of cells adsorbed to nematic tactoids (at 33°C) ($N = 35$) and isotropic tactoids (at 30°C) ($N = 37$) following a 15 min equilibration period at the indicated temperature. The tactoids were of similar size: ~30 μm in diameter. Error bars represent standard errors.

time on the N-I interface of nematic tactoids relative to isotropic tactoids. These differences provide added support for the conclusion that the elasticity of the nematic phase generates a barrier for bacterial detachment and that, in the presence of this barrier, bacteria escape is largely limited to a structured pathway that involves director-guided motion to boojums through which the cells exit using a force generated by a multicellular assembly.

Capture and release of motile bacteria by using nematic elasticity and topological defects

Our observations of the infrequency with which bacteria escape from the N-I interface of isotropic tactoids into the nematic phase—particularly when not proximate to a topological defect—led us to explore if it is possible to corral motile *P. mirabilis* within large isotropic domains of a 15 wt % DSCG solution at 30°C by quenching the solution from the isotropic phase into the biphasic region rather than heating from the nematic (the latter was shown in Fig. 3). We also hypothesized that the probability of encountering a topological defect would be dependent on domain size and thus release of bacteria from isotropic corrals might be tuned via control of the size of domains. To test this concept, we heated a suspension of cells in DSCG to 40°C and subsequently quenched the sample to 30°C. As the DSCG solution entered the biphasic region during cooling, motile cells were excluded from nucleating nematic phase tactoids. While the sample was equilibrated at 30°C, the nematic tactoids grew in size and coalesced, trapping isotropic phase domains (Fig. 5, *A–C*). These isotropic domains were initially larger (~60 μm in diameter) than the sessile tactoid domains described previously (Figs. 1 and 3) and contacted the glass substrates on both sides of the 18-μm tall chamber. As these large isotropic domains

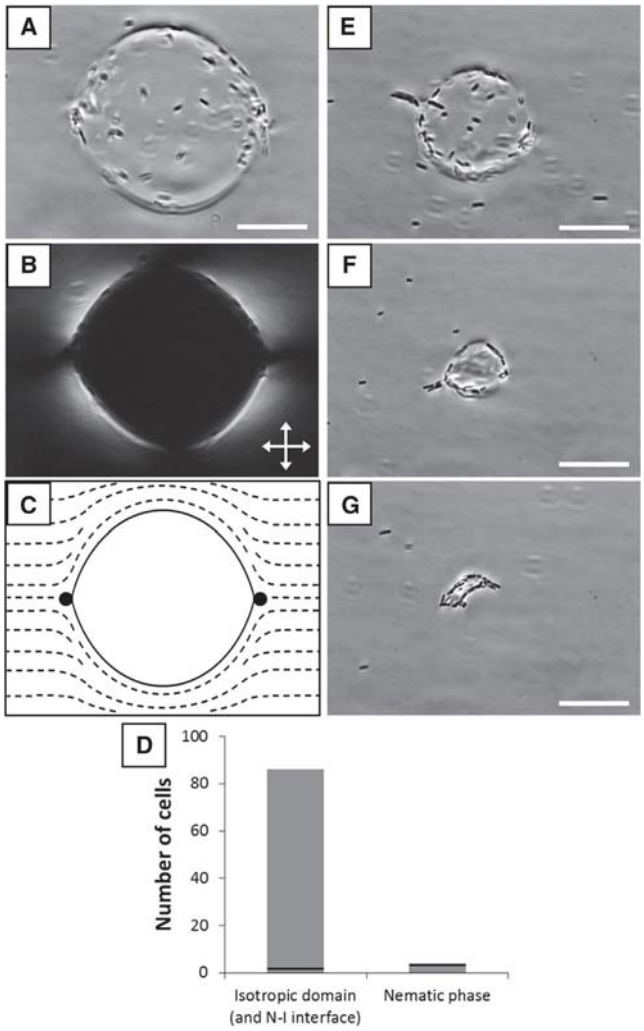

FIGURE 5 Temperature-controlled capture and release of bacteria from an isotropic domain. (*A*) Bright field micrograph of an isotropic domain (diameter ~60 μm) that forms upon quenching a 15 wt % DSCG sample from 40°C to 30°C and spans the 18 μm-thick imaging chamber. (*B*) Corresponding crossed polars optical micrograph. (*C*) Schematic representation of the director profile corresponding to a cross section of the isotropic domain imaged in *A* and *B*. (*D*) Number of cells trapped by the isotropic domain depicted in *A* and in the nematic phase encompassing it. Cells both in and out of the focal plane are counted. The black, horizontal lines indicate the number of cells expected to be in the isotropic and nematic domains within the field of view as calculated based on the total concentration of cells (~10^5 cells/μL) in the suspension. (*E–G*) Bright field micrographs of the isotropic sample after cooling to 29.5°C, 29.2°C, and 29°C, respectively. Rafts of cells collectively escape into the nematic phase in *E* and *F*, whereas an aggregate of cells forms as the isotropic domain in *G* nearly disappears. Scale bars are 20 μm.

formed, the inward-directed motion of the N-I interface pushed high densities of cells forward and trapped them within or at the domain interface (Fig. 5 *A*, Movie S4). For example, we observed that >80 cells were captured within the 60 μm-wide isotropic domain near the plane of focus depicted in Fig. 5 *A*, representing an enhancement in the local concentration of the bacteria (Fig. 5 *D*).

Due to the orientation of the director profile in the adjacent nematic phase (see Fig. 5 *C*), motile cells were largely constrained to circular trajectories when adsorbed to the interface of the nearly cylindrical isotropic domains with diameters of 35 μm or larger. The large size and nearly circular cross section of these isotropic domains (such as the one depicted in Fig. 5 *A*) prevented most of the cells from escaping into the nematic phase. The cells were, in effect, corralled by the elasticity of the surrounding nematic phase. The few escape events that did occur took place proximate to one of the two LC surface defects in the nematic phase near the poles of the spanning isotropic domains (Fig. 5 *C*), which are either boojums or cross sections of disclination lines.

By adjusting the temperature of the sample, we were able to tune the size of the isotropic corrals in which cells were confined. Specifically, over the course of 20 min, we slowly lowered the temperature of the sample from 30°C to 29°C and observed the isotropic domain to reduce in size and transform into a sessile droplet (Fig. 5, *E* and *F*). We found that by decreasing the area of the interface between the nematic and isotropic phases, *P. mirabilis* cells more frequently encountered the topological defects at the cusped regions at the N-I interface and escaped in greater numbers. For example, in the specific experiment highlighted in Fig. 5, when the isotropic domain was ~30 μm in diameter (Fig. 5 *E*), we observed that 20 cells escaped into the nematic phase over the course of 1 min, representing an increase in escape frequency of nearly 4 times over when the domain was between 35 and 60 μm in diameter. This increase in escape frequency may also reflect changes in the morphology of the N-I interface near the LC surface defects that occur as the isotropic domain becomes smaller and transforms into a sessile state (with two boojums, similar to Fig. 3).

Over the course of the experiment, not all of the cells escaped from the isotropic domain. We hypothesize that this is the result of the rate of shrinkage of the isotropic domain exceeding the rate at which bacteria escape via the cusps at the chosen experimental conditions. When the temperature of our sample reached 29°C, we observed the cells that remained adsorbed to the interface of the shrinking isotropic domain to ultimately form a small multicellular aggregate (Fig. 5 *G*). Individual cells seldom escaped from aggregates formed in this manner, as the close packing of cells may reduce their ability to generate flagella-derived propulsive forces. Past studies have reported that cooling DSCG samples from the biphasic region into the homogeneous nematic phase can shrink isotropic domains to disclination cores that remain stable even when positioned deep within the nematic phase (50). The disclination cores serve as the sites of nucleation of isotropic tactoids upon reheating. We also observed an isotropic tactoid to reform at the site of the bacterial aggregate in Fig. 5 *G* upon reheating.

DISCUSSION

The results presented in this work reveal that interfacial environments defined by anisotropic phases have a profound impact on fundamental behaviors of motile bacteria. Our observations have broad implications for studies aimed at understanding microbes in a range of ecologically and pathogenically relevant microenvironments that are known or suspected to be anisotropic. Specifically, we have found that motile *P. mirabilis* cells adsorbed at interfaces between coexisting nematic and isotropic phases of a biocompatible lyotropic LC are oriented by the elasticity of the LC, resulting in strongly biased motion of motile bacteria along the interfacial director profile of tactoids. Additional evidence of the influence of the nematic elasticity of the N-I interface can be found in our observations of multicellular behaviors (Fig. 6). In particular, we observed *P. mirabilis* cells to assemble into linear chains induced by LC elasticity at the N-I interface (Fig. 6, *B* and *C*). These chains were observed to be dynamic and reversible consistent with the interplay between LC elasticity-mediated forces and flagella-derived propulsive forces (48) (Fig. 6, *D* and *E*). These observations suggest that elastic strain associated with anisotropic interfacial environments can orient rod-shaped bacteria and lead to new, to our knowledge, classes of interbacterial interactions that are absent in isotropic interfacial environments.

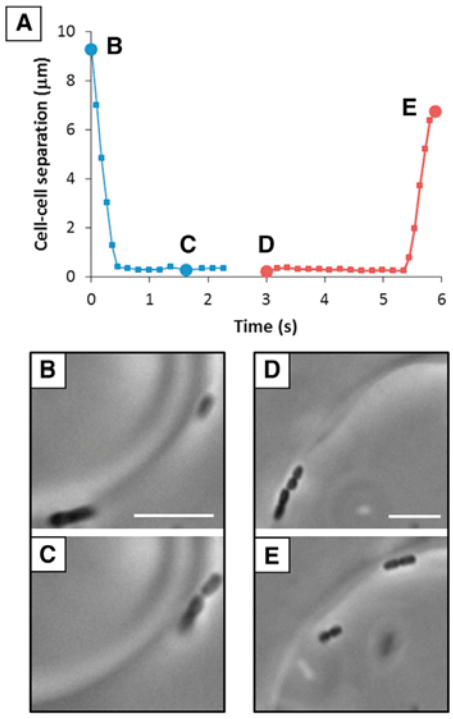

FIGURE 6 Reversible formation of multicellular assemblies at the N-I interface. (*A*) Estimated minimum separation distance as a function of time between (*B* and *C*) two motile *P. mirabilis* cells that undergo LC elasticity-mediated end-on-end association and between (*D* and *E*) two motile *P. mirabilis* cells that dissociate from a chain-like assembly. Scale bars are 5 μm. To see this figure in color, go online.

Another key influence of the elasticity of the nematic phase on the behavior of the bacteria at the N-I interface was evident in the statistics of bacterial populations found at the interfaces of isotropic versus nematic tactoids. Specifically, we observed the elastic energy penalty associated with strain of the LC about the cells in the nematic phase to substantially influence the probability of escape from nematic and isotropic domains. Moreover, the barrier created by the elastic energy penalty resulted in the cells adopting a cooperative mechanism of escape that involved formation of transient colonies at the poles of isotropic domains. This set of observations suggests that individual bacteria present at an interface between an isotropic and anisotropic microenvironment in a biofilm, for example, will tend to preferentially exit the interface into the isotropic domain. However, formation of multicellular assemblies may enable the bacteria to inhabit the anisotropic domain.

One of the most interesting findings of our study relates to the role that topological defects play in mediating the escape of bacteria from the N-I interface, particularly escape into bulk nematic phases. We observed escape from isotropic tactoids to occur most commonly through a collective mechanism that involved three distinct steps: i), director-guided motion of motile cells to a boojum; ii), trapping of individual bacteria at the boojum; iii), cooperative escape of an assembly of bacteria from the boojum once a critical colony size was formed. This collective phenomenon is in contrast to that observed for escape from the N-I interface into the isotropic phase of DSCG. Although the predominant mechanism of escape was still via a boojum, individual bacteria were able to dissociate from the potential well caused by the defect. In addition, nonmotile bacteria were observed to associate irreversibly at the boojums of tactoids (Fig. S4), similar to passive synthetic particles. More broadly, these results suggest that defects present in anisotropic native environments in which bacteria live, whether transient or equilibrium in nature, likely play a central role in dictating fundamental behaviors, including collective dynamic behaviors, of the cells.

In a recent publication, Zhou et al. describe an observation of a single *B. subtilis* cell moving along the interface of an isotropic tactoid in a nematic LC before escaping attachment to the interface into the LC at the cusp of the tactoid (49). We note that this observation contrasts with our own conclusions obtained with *P. mirabilis* cells in which we quantified the statistics of escape and found escape from isotropic tactoids to be most commonly mediated by the cooperative multicellular mechanism described previously (Fig. 3 *E*). We also note that Zhou et al. do not report evidence of elasticity-mediated interactions between *B. subtilis* cells as we reported previously in bulk LCs (48), suggesting that *P. mirabilis* and *B. subtilis* cells differ in fundamental ways in terms of their behavior in LCs and at LC interfaces. Additionally, although both *P. mirabilis* and *B. subtilis* move at similar velocities through nematic

DSCG (8.8 ± 0.2 μm/s (48) and 8 ± 3 μm/s (49), respectively), *B. subtilis* cells likely generate greater propulsive forces because they are approximately twice as long as *P. mirabilis*. Thus, although we have found that flagella-derived propulsive forces and elasticity-mediated forces are comparable in magnitude for *P. mirabilis* cells in DSCG (48), the relative magnitude of these forces appears to be different for *B. subtilis*.

We end this discussion by noting that the influence of nematic elasticity and topological defects on dynamic interfacial behaviors of bacteria, as reported in this work, also suggests the basis of new, to our knowledge, approaches to manipulating bacteria in a technological context. We show, for example, that it is possible to use nematic elasticity of LCs to corral motile cells within isotropic domains in a continuous nematic phase and to alter the frequency with which cells escape through the topological defects of the domains via tuning of the sizes of the domain. In future studies, we envision spatially targeted heating of a suspension of cells in DSCG (e.g., using Joule heating from an embedded wire or by dispersing dye molecules in the sample and employing a focused beam of light) to dynamically control the localization and release of bacteria.

CONCLUSION

Overall, our observations provide fundamental insight into how anisotropy, nematic elastic forces, and topological defects can substantially change the behaviors of motile bacteria at interfaces between isotropic and anisotropic microenvironments in ways that are not observed at interfaces between isotropic phases. Not only do we find that the dynamics of individual cells are altered at anisotropic LC interfaces, as demonstrated by the guided motion of cells along the nematic director and interactions of cells with boojums, but we also uncover multicellular phenomena that emerge, including the organization of cells into chains and the formation and cooperative escape of large assemblies of cells from interfaces of isotropic domains. These studies open a new window through which to view the behavior of bacteria in conditions that recapitulate key physical properties of native bacterial environments and also suggest new opportunities to achieve temporal and spatial control over bacteria.

SUPPORTING MATERIAL

Six figures and four movies are available at http://www.biophysj.org/biophysj/supplemental/S0006-3495(14)00466-4.

This work was supported by the National Science Foundation (under awards DMR-1121288 (MRSEC), CBET-0754921, and MCB-1120832), the National Institutes of Health (CA108467, AI092004, and 5T32GM08349), the Army Research Office (W911-NF-11-1-0251 and W911-NF-14-1-0140), and the United States Department of Agriculture (WIS01594).

N.L.A. declares a significant financial interest in Platypus Technologies LLC, a for-profit company that has developed LC-based technologies for molecular analysis.

REFERENCES

1. Lens, P., A. P. Moran, T. Mahony, P. Stoodley, and V. O'Flaherty, editors. 2003. Biofilms in Medicine, Industry and Environmental Biotechnology: Characteristics, Analysis and Control. IWA Publishing, London, UK.
2. Parsek, M. R., and P. K. Singh. 2003. Bacterial biofilms: an emerging link to disease pathogenesis. *Annu. Rev. Microbiol.* 57:677–701.
3. Hall-Stoodley, L., J. W. Costerton, and P. Stoodley. 2004. Bacterial biofilms: from the natural environment to infectious diseases. *Nat. Rev. Microbiol.* 2:95–108.
4. Hallam, N. B., J. R. West, …, J. Simms. 2001. The potential for biofilm growth in water distribution systems. *Water Res.* 35:4063–4071.
5. Oostdijk, E. A. N., A. M. G. A. de Smet, …, M. J. M. Bonten. 2010. Ecological effects of selective decontamination on resistant gram-negative bacterial colonization. *Am. J. Respir. Crit. Care Med.* 181:452–457.
6. Chmielewski, R. A. N., and J. F. Frank. 2003. Biofilm formation and control in food processing facilities. *Compr. Rev. Food Sci. Food Saf.* 2:22–32.
7. Shi, X., and X. Zhu. 2009. Biofilm formation and food safety in food industries. *Trends Food Sci. Technol.* 20:407–413.
8. Johansson, J. F., L. R. Paul, and R. D. Finlay. 2004. Microbial interactions in the mycorrhizosphere and their significance for sustainable agriculture. *FEMS Microbiol. Ecol.* 48:1–13.
9. Evans, F. F., A. S. Rosado, …, L. Seldin. 2004. Impact of oil contamination and biostimulation on the diversity of indigenous bacterial communities in soil microcosms. *FEMS Microbiol. Ecol.* 49:295–305.
10. Guarner, F., and J.-R. Malagelada. 2003. Gut flora in health and disease. *Lancet.* 361:512–519.
11. Flint, H. J., S. H. Duncan, …, P. Louis. 2007. Interactions and competition within the microbial community of the human colon: links between diet and health. *Environ. Microbiol.* 9:1101–1111.
12. DiLuzio, W. R., L. Turner, …, G. M. Whitesides. 2005. *Escherichia coli* swim on the right-hand side. *Nature.* 435:1271–1274.
13. Lauga, E., W. R. DiLuzio, …, H. A. Stone. 2006. Swimming in circles: motion of bacteria near solid boundaries. *Biophys. J.* 90:400–412.
14. Berke, A. P., L. Turner, …, E. Lauga. 2008. Hydrodynamic attraction of swimming microorganisms by surfaces. *Phys. Rev. Lett.* 101:038102.
15. Lauga, E., and T. R. Powers. 2009. The hydrodynamics of swimming microorganisms. *Rep. Prog. Phys.* 72:096601.
16. Lemelle, L., J.-F. Palierne, …, C. Place. 2010. Counterclockwise circular motion of bacteria swimming at the air-liquid interface. *J. Bacteriol.* 192:6307–6308.
17. Morse, M., A. Huang, …, J. X. Tang. 2013. Molecular adsorption steers bacterial swimming at the air/water interface. *Biophys. J.* 105:21–28.
18. Flemming, H.-C. 2002. Biofouling in water systems—cases, causes and countermeasures. *Appl. Microbiol. Biotechnol.* 59:629–640.
19. del Pozo, J. L., and R. Patel. 2007. The challenge of treating biofilm-associated bacterial infections. *Clin. Pharmacol. Ther.* 82:204–209.
20. Høiby, N., T. Bjarnsholt, …, O. Ciofu. 2010. Antibiotic resistance of bacterial biofilms. *Int. J. Antimicrob. Agents.* 35:322–332.
21. Klapper, I., C. J. Rupp, …, P. Stoodley. 2002. Viscoelastic fluid description of bacterial biofilm material properties. *Biotechnol. Bioeng.* 80:289–296.
22. Shaw, T., M. Winston, …, P. Stoodley. 2004. Commonality of elastic relaxation times in biofilms. *Phys. Rev. Lett.* 93:098102.
23. Hohne, D. N., J. G. Younger, and M. J. Solomon. 2009. Flexible microfluidic device for mechanical property characterization of soft viscoelastic solids such as bacterial biofilms. *Langmuir.* 25:7743–7751.

24. Flemming, H.-C., and J. Wingender. 2010. The biofilm matrix. *Nat. Rev. Microbiol.* 8:623–633.
25. Pavlovsky, L., J. G. Younger, and M. J. Solomon. 2013. In situ rheology of *Staphylococcus epidermidis* bacterial biofilms. *Soft Matter.* 9:122–131.
26. Hwang, S. H., M. Litt, and W. C. Forsman. 1969. Rheological properties of mucus. *Rheol. Acta.* 8:438–448.
27. Tam, P. Y., D. F. Katz, and S. A. Berger. 1980. Non-linear viscoelastic properties of cervical mucus. *Biorheology.* 17:465–478.
28. Madoff, L. C., S. J. Thaler, and J. H. Maguire. 2005. Infectious arthritis. *In* Harrison's Principles of Internal Medicine, 16th ed.. A. S. Fauci, D. L. Kasper, S. L. Hauser, D. L. Longo, and J. L. Jameson, editors. McGraw-Hill, New York, pp. 2050–2055.
29. Stokes, J. R., and G. A. Davies. 2007. Viscoelasticity of human whole saliva collected after acid and mechanical stimulation. *Biorheology.* 44:141–160.
30. Haward, S. J., J. A. Odell, …, T. Hall. 2011. Extensional rheology of human saliva. *Rheol. Acta.* 50:869–879.
31. Rey, A. D. 2010. Liquid crystal models of biological materials and processes. *Soft Matter.* 6:3402–3429.
32. Houry, A., M. Gohar, …, R. Briandet. 2012. Bacterial swimmers that infiltrate and take over the biofilm matrix. *Proc. Natl. Acad. Sci. USA.* 109:13088–13093.
33. Mudd, S., and E. B. H. Mudd. 1924. The penetration of bacteria through capillary spaces. IV. A kinetic mechanism in interfaces. *J. Exp. Med.* 40:633–645.
34. Mudd, S., and E. B. H. Mudd. 1924. Certain interfacial tension relations and the behavior of bacteria in films. *J. Exp. Med.* 40:647–660.
35. Rosenberg, M., D. Gutnick, and E. Rosenberg. 1980. Adherence of bacteria to hydrocarbons: a simple method for measuring cell-surface hydrophobicity. *FEMS Microbiol. Lett.* 9:29–33.
36. Rosenberg, M. 1984. Bacterial adherence to hydrocarbons: a useful technique for studying cell surface hydrophobicity. *FEMS Microbiol. Lett.* 22:289–295.
37. Kang, Z., A. Yeung, …, M. R. Gray. 2008. Hydrophobic bacteria at the hexadecane-water interface: examination of micrometre-scale interfacial properties. *Colloids Surf. B Biointerfaces.* 67:59–66.
38. Lin, I.-H., G. M. Koenig, Jr., …, N. L. Abbott. 2008. Ordering of solid microparticles at liquid crystal-water interfaces. *J. Phys. Chem. B.* 112:16552–16558.
39. Koenig, Jr., G. M., I.-H. Lin, and N. L. Abbott. 2010. Chemoresponsive assemblies of microparticles at liquid crystalline interfaces. *Proc. Natl. Acad. Sci. USA.* 107:3998–4003.
40. Smalyukh, I. I., S. Chernyshuk, …, O. D. Lavrentovich. 2004. Ordered droplet structures at the liquid crystal surface and elastic-capillary colloidal interactions. *Phys. Rev. Lett.* 93:117801.
41. Nazarenko, V. G., A. B. Nych, and B. I. Lev. 2001. Crystal structure in nematic emulsion. *Phys. Rev. Lett.* 87:075504.
42. Gharbi, M. A., M. Nobili, …, C. Blanc. 2011. Behavior of colloidal particles at a nematic liquid crystal interface. *Soft Matter.* 7:1467–1471.
43. Abras, D., G. Pranami, and N. L. Abbott. 2012. The mobilities of micro- and nano-particles at interfaces of nematic liquid crystals. *Soft Matter.* 8:2026–2035.
44. Mondiot, F., X. Wang, …, N. L. Abbott. 2013. Liquid crystal-based emulsions for synthesis of spherical and non-spherical particles with chemical patches. *J. Am. Chem. Soc.* 135:9972–9975.
45. Whitmer, J. K., X. Wang, …, J. J. de Pablo. 2013. Nematic-field-driven positioning of particles in liquid crystal droplets. *Phys. Rev. Lett.* 111:227801.
46. Tuson, H. H., M. F. Copeland, …, D. B. Weibel. 2013. Flagellum density regulates *Proteus mirabilis* swarmer cell motility in viscous environments. *J. Bacteriol.* 195:368–377.
47. Kumar, A., T. Galstian, …, S. Rainville. 2013. The motility of bacteria in an anisotropic liquid environment. *Mol. Cryst. Liq. Cryst. (Phila. Pa.).* 574:33–39.
48. Mushenheim, P. C., R. R. Trivedi, …, N. L. Abbott. 2014. Dynamic self-assembly of motile bacteria in liquid crystals. *Soft Matter.* 10:88–95.
49. Zhou, S., A. Sokolov, …, I. S. Aranson. 2014. Living liquid crystals. *Proc. Natl. Acad. Sci. USA.* 111:1265–1270.
50. Kim, Y.-K., S. V. Shiyanovskii, and O. D. Lavrentovich. 2013. Morphogenesis of defects and tactoids during isotropic-nematic phase transition in self-assembled lyotropic chromonic liquid crystals. *J. Phys. Condens. Matter.* 25:404202.
51. Prinsen, P., and P. van der Schoot. 2003. Shape and director-field transformation of tactoids. *Phys. Rev. E Stat. Nonlin. Soft Matter Phys.* 68:021701.
52. Nastishin, Y. A., H. Liu, …, O. D. Lavrentovich. 2005. Optical characterization of the nematic lyotropic chromonic liquid crystals: light absorption, birefringence, and scalar order parameter. *Phys. Rev. E Stat. Nonlin. Soft Matter Phys.* 72:041711.
53. van Bijnen, R. M. W., R. H. J. Otten, and P. van der Schoot. 2012. Texture and shape of two-dimensional domains of nematic liquid crystals. *Phys. Rev. E Stat. Nonlin. Soft Matter Phys.* 86:051703.
54. Nastishin, Y. A., H. Liu, …, M. A. Anisimov. 2004. Pretransitional fluctuations in the isotropic phase of a lyotropic chromonic liquid crystal. *Phys. Rev. E Stat. Nonlin. Soft Matter Phys.* 70:051706.
55. Champion, J. V., and G. H. Meeten. 1973. Conformation of sodium cromolyn in aqueous solution using light scattering and magnetic birefringence. *J. Pharm. Sci.* 62:1589–1595.
56. Luk, Y.-Y., M. L. Tingey, …, N. L. Abbott. 2003. Using liquid crystals to amplify protein−receptor interactions: design of surfaces with nanometer-scale topography that present histidine-tagged protein receptors. *Langmuir.* 19:1671–1680.
57. Kaznacheev, A. V., M. M. Bogdanov, and S. A. Taraskin. 2002. The nature of prolate shape of tactoids in lyotropic inorganic liquid crystals. *J. Exp. Theor. Phys.* 95:57–63.
58. Kaznacheev, A. V., M. M. Bogdanov, and A. S. Sonin. 2003. The influence of anchoring energy on the prolate shape of tactoids in lyotropic inorganic liquid crystals. *J. Exp. Theor. Phys.* 97:1159–1167.
59. Volovik, G. E., and O. D. Lavrentovich. 1983. Topological dynamics of defects: boojums in nematic drops. *Sov. Phys. JETP.* 58:1159–1166.
60. Nastishin, Y. A., K. Neupane, …, S. Sprunt. 2008. Elasticity and viscosity of a lyotropic chromonic nematic studied with dynamic light scattering. Electronic-Liquid Crystal Communications. arXiv.org/abs/0807.2669.
61. Prinsen, P., and P. van der Schoot. 2004. Parity breaking in nematic tactoids. *J. Phys. Condens. Matter.* 16:8835–8850.
62. Tortora, L., and O. D. Lavrentovich. 2011. Chiral symmetry breaking by spatial confinement in tactoidal droplets of lyotropic chromonic liquid crystals. *Proc. Natl. Acad. Sci. USA.* 108:5163–5168.
63. Chen, W., and D. G. Gray. 2002. Interfacial tension between isotropic and anisotropic phases of a suspension of rodlike particles. *Langmuir.* 18:633–637.
64. Binks, B. P., and T. S. Horozov. 2006. Colloidal particles at liquid interfaces: an introduction. *In* Colloidal Particles at Liquid Interfaces. B. P. Binks and T. S. Horozov, editors. Cambridge University Press, Cambridge, pp. 1–15.
65. Smalyukh, I. I., J. Butler, …, G. C. L. Wong. 2008. Elasticity-mediated nematiclike bacterial organization in model extracellular DNA matrix. *Phys. Rev. E Stat. Nonlin. Soft Matter Phys.* 78:030701.
66. West, J. L., A. Glushchenko, …, M. P. Allen. 2002. Drag on particles in a nematic suspension by a moving nematic-isotropic interface. *Phys. Rev. E Stat. Nonlin. Soft Matter Phys.* 66:012702.
67. Loudet, J. C., and B. Pouligny. 2011. How do mosquito eggs self-assemble on the water surface? *Eur. Phys. J. E Soft Matter.* 34:76.